

PAPER • OPEN ACCESS


Universal quantum computation and quantum error correction with ultracold atomic mixtures

To cite this article: Valentin Kasper *et al* 2022 *Quantum Sci. Technol.* **7** 015008

View the [article online](#) for updates and enhancements.

You may also like

- [4th International Colloquium on Atomic Spectra and Oscillator Strengths for Astrophysical and Laboratory Plasmas](#)
David S Leckrone and Jack Sugar
- [Imaging Atomic Structure, Strain, and Disorder By Atomic Electron Tomography](#)
Peter Ercius, Jihan Zhou, Yongsoo Yang et al.
- [Heavy-Ion Spectroscopy and QED Effects in Atomic Systems](#)
Ingvar Lindgren, Indrek Martinson and Reinhold Schuch

 **kiutra**

Easy-to-use and Helium-3 free
cryogenics solutions

LEARN MORE

Quantum Science and Technology



PAPER

Universal quantum computation and quantum error correction with ultracold atomic mixtures

OPEN ACCESS

RECEIVED
8 June 2021

REVISED
10 September 2021










ACCEPTED FOR PUBLICATION
6 October 2021

PUBLISHED
11 November 2021

Original content from this work may be used under the terms of the [Creative Commons Attribution 4.0 licence](https://creativecommons.org/licenses/by/4.0/).

Any further distribution of this work must maintain attribution to the author(s) and the title of the work, journal citation and DOI.



Valentin Kasper^{1,*} , Daniel González-Cuadra¹ , Apoorva Hegde² , Andy Xia² , Alexandre Dauphin¹ , Felix Huber¹ , Eberhard Tiemann³, Maciej Lewenstein^{1,4} , Fred Jendrzejewski²  and Philipp Hauke⁵ 

¹ ICFO-Institut de Ciències Fòniques, The Barcelona Institute of Science and Technology, Av. Carl Friedrich Gauss 3, 08860 Barcelona, Spain

² Universität Heidelberg, Kirchoff-Institut für Physik, Im Neuenheimer Feld 227, 69120 Heidelberg, Germany

³ Institut für Quantenoptik, Leibniz Universität Hannover, 30167 Hannover, Germany

⁴ ICREA, Pg. Lluís Companys 23, 08010 Barcelona, Spain

⁵ INO-CNR BEC Center and Department of Physics, University of Trento, Via Sommarive 14, I-38123 Trento, Italy

* Author to whom any correspondence should be addressed.

E-mail: valentin.kasper@icfo.eu

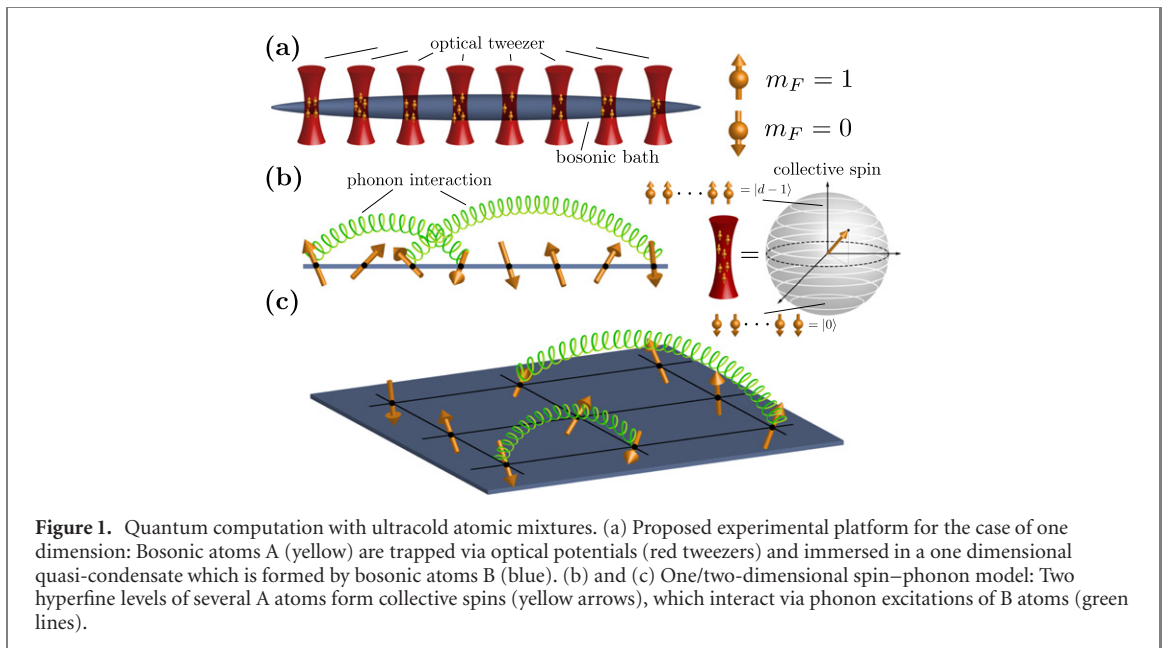
Keywords: ultracold atoms, quantum computation, atomic mixtures, quantum error correction

Abstract

Quantum information platforms made great progress in the control of many-body entanglement and the implementation of quantum error correction, but it remains a challenge to realize both in the same setup. Here, we propose a mixture of two ultracold atomic species as a platform for universal quantum computation with long-range entangling gates, while providing a natural candidate for quantum error-correction. In this proposed setup, one atomic species realizes localized collective spins of tunable length, which form the fundamental unit of information. The second atomic species yields phononic excitations, which are used to entangle collective spins. Finally, we discuss a finite-dimensional version of the Gottesman–Kitaev–Preskill code to protect quantum information encoded in the collective spins, opening up the possibility to universal fault-tolerant quantum computation in ultracold atom systems.

Quantum information processing is expected to show fundamental advantages over classical approaches to computation, simulation, and communication [1]. To exploit these advantages, both the efficient creation of entanglement and the correction of errors are essential [2, 3]. There have been spectacular advancements in the field of synthetic quantum devices, which allow for controlled many-body entanglement [4–6] or the implementation of quantum error correction (QEC) [7–10]. However, it is still a challenge to design a quantum computation platform that efficiently realizes both features simultaneously. Here, we propose to use a mixture of two ultracold atomic species to implement a universal quantum computer, permitting long-range entangling gates as well as QEC (see figure 1). One atomic species forms localized collective spins, which can be fully controlled and represent the basic units of information. The second species is used for the generation of pairwise entanglement of the collective spins, resulting in a universal gate set. Moreover, we illustrate how to encode a logical qubit in the collective spin, how to detect and correct errors, and present a universal gate set on the logical qubits. Altogether, this opens a new possibility for quantum computation with error correction in ultracold atomic systems, presenting a significant step toward fault-tolerant quantum computation.

The proposal of this work complements existing platforms such as nuclear magnetic resonance [11], nitrogen-vacancy centers in diamonds [12], photonics [13], silicon based qubits [14], superconducting qubits [15], and trapped ions [16]. One key challenge in many of these platforms is to reduce the technical overhead when synthesizing long-range gates out of short range gates, as it happens, e.g. in superconducting qubit experiments. While trapped ion systems provide efficient long-range entangling gates, they face technical challenges in establishing full control beyond one hundred ions [17, 18]. Furthermore, many implementations of QEC demand a considerable number of physical qubits to store one logical qubit, and



additional control qubits for the encoding, decoding, and correcting processes [19]. Whereas the challenges of efficient long-range entanglement and QEC appear daunting, ultracold atomic mixtures may provide a solution for both.

Ultracold atoms have become a major quantum simulation platform to solve problems in the field of condensed-matter [20–22] and high-energy physics [23–27]. Yet, even though universal quantum information processing with ultracold atom systems was investigated conceptually, the experimental implementations remain elusive [28–30]. The realization of gates with high-fidelity and the ability to apply sequences of several gates is particularly challenging. However, recent progress in systems of atoms trapped in optical lattices or optical tweezers has made it possible to realize large quantum many-body systems [31] with fast, high-fidelity entangling gates [32, 33]. Simultaneously, multi-component Bose–Einstein condensates were used to form large collective spins [34–38] and spatially distribute entanglement via expansion [39]. Ultracold atomic mixtures allow for other entanglement mechanisms such as phonon induced interactions [40–43], or particle mediation [29]. The effect of phonons on a single atomic species has already been experimentally studied in the context of polaron physics [44, 45].

We first introduce the fundamental unit of information of our platform: collective spins of controllable length. They are realized by condensing bosonic atoms into a single spatial mode of an optical tweezer. The remaining degrees of freedom are two internal states of the atoms, which can be described using a collective spin. The length of the collective spin is controlled by the number of trapped atoms enabling access to the qubit, qudit, and continuous variable regime. The collective occupation of the internal degrees of freedom constitute the computational basis. By tuning the length of the collective spin, quantum information processing can be done with qubits, qudits or continuous variables. The atoms within a tweezer can be reliably prepared in a fully polarized state, which then acts as the initial state of the computation. A single collective spin can be fully controlled locally via linear operations such as Raman coupling, and non-linear operations such as the interaction between the atoms in different hyperfine states.

In order to create entanglement between the collective spins, we employ a second atomic species, which forms a bosonic bath with phononic excitations. The contact interaction between the two atomic species gives rise to the exchange of phononic excitations between the collective spins. The resulting long-range interaction permits an efficient generation of entanglement between distant spins. The operations on a single collective spin in combination with their pairwise entanglement forms a universal gate set. The gate speed is expected to be much faster than the decoherence time in the platform suggested here. Altogether, this platform fulfills DiVincenzo’s criteria for quantum computation [46].

Moreover, we illustrate a scheme for QEC based on the stabilizer formalism. The method encodes a logical qubit into superpositions of states within the higher dimensional Hilbert space of the collective spin. We further explain how to prepare, detect and correct specific errors by using additional control qubits. Finally, we present a universal gate set for the logical qubits.

This work is organized as follows. In section 1, we explain how one atomic species forms a collective spin and how to generate arbitrary unitaries on such a single object. In section 2, we discuss the interaction between the collective spins and a phonon bath, and how this can be used to entangle two collective spins,

which then can be employed for universal quantum computation. In section 3, we discuss the state preparation and readout of the collective spins. In section 4, we lie out the experimental characteristics of this quantum computation platform. Finally, in section 5 we discuss how to implement QEC.

1. Collective spins

In this section, we discuss the fundamental unit of information of our proposal: a collective spin with controllable length. In order to realize such a collective spin we consider bosonic atoms of type A, which are localized at the local minima \mathbf{y} of the optical potential, e.g. arrays of optical tweezer or an optical lattice (see figure 1(a)). The annihilation (creation) operators of the atoms on site \mathbf{y} are $a_m(\mathbf{y})$ and $a_m^\dagger(\mathbf{y})$, where m indicates the two internal states (0, 1) of the atom. The local confining potential is chosen such that there is no hopping. Hence, the atom number per site $N_A(\mathbf{y}) = a_1^\dagger(\mathbf{y})a_1(\mathbf{y}) + a_0^\dagger(\mathbf{y})a_0(\mathbf{y})$ is conserved [47] and the atoms form a collective spin via the Schwinger representation:

$$L_z(\mathbf{y}) = \frac{1}{2}[a_1^\dagger(\mathbf{y})a_1(\mathbf{y}) - a_0^\dagger(\mathbf{y})a_0(\mathbf{y})], \quad (1a)$$

$$L_+(\mathbf{y}) = a_1^\dagger(\mathbf{y})a_0(\mathbf{y}), \quad (1b)$$

$$L_-(\mathbf{y}) = a_0^\dagger(\mathbf{y})a_1(\mathbf{y}), \quad (1c)$$

with $L_x(\mathbf{y}) = [L_+(\mathbf{y}) + L_-(\mathbf{y})]/2$ and $L_y(\mathbf{y}) = (-i)[L_+(\mathbf{y}) - L_-(\mathbf{y})]/2$. The conservation of atom number per site determines also the magnitude of the angular momentum $\ell = N_A/2$. The eigenstates of the L_z operator are denoted by $|m_\ell\rangle$ with m_ℓ being an integer or half-integer ranging from $m_\ell = -\ell, \dots, \ell$. By defining the computational basis $|j\rangle \equiv |-\ell + j\rangle$ with $j = 0, \dots, N_A$ a collective spin can be interpreted as a qudit with dimension $d = N_A + 1$. Moreover, we can access the qubit ($N_A = 1$), qudit ($N_A > 1$), and continuous variable ($N_A \rightarrow \infty$) regime by tuning the atom number per site. In particular, the Hilbert space dimension of a single collective spins scales linearly with the numbers of atoms.

In order to realize unitary operations acting on a single collective spin, we consider the time evolution generated by the Hamiltonian

$$H_A = \sum_{\mathbf{y}} [\chi(\mathbf{y})L_z^2(\mathbf{y}) + \Delta(\mathbf{y})L_z(\mathbf{y}) + \Omega(\mathbf{y})L_x(\mathbf{y})]. \quad (2)$$

As detailed in appendix A, this Hamiltonian can be implemented by a two component Bose gas localized in optical tweezers, where the first term corresponds to the interaction between the atoms, the second is due to the presence of the magnetic field, and the third term to a Rabi coupling between the hyperfine states. The interactions between the atoms are described by $L_z^2(\mathbf{y}) = \frac{1}{4}[n_1^2(\mathbf{y}) + n_0^2(\mathbf{y}) - 2n_0(\mathbf{y})n_1(\mathbf{y})]$, which involve both spin-states, but no spin-changing collisions.

The Hamiltonian in equation (2) can generate all unitary operations on a single collective spin since all couplings $\chi(\mathbf{y})$, $\Delta(\mathbf{y})$, and $\Omega(\mathbf{y})$ can be switched on and off independently on each site in ultracold atom systems [48]. For the $F = 1$ hyperfine manifold, the coupling $\chi(\mathbf{y}) = 0$ can be achieved by hosting the atoms in the magnetic substates $m_F = 1$ and $m_F = -1$, while $\chi(\mathbf{y}) \neq 0$ when the atoms are in the magnetic substates $m_F = 1$ and $m_F = 0$. The switching of $\chi(\mathbf{y})$ was illustrated in the context of mixture experiments in a recent work using Raman transitions [49]. A great advantage of using laser addressing is that the magnetic field does not have to be controlled at the μm scale, which is the typical separation of optical tweezers. Similarly, the couplings $\Omega(\mathbf{y})$ and $\Delta(\mathbf{y})$ can be tuned via Raman coupling in the same way as in the high-fidelity implementations with trapped ions [50].

For the qubit case ($d = N_A + 1 = 2$), the operators L_x and L_z together with the identity $\mathbf{1}$ suffice to obtain all $U(2)$ transformations [51]. For qudits ($d = N_A + 1 > 2$) the additional non-linear operation L_z^2 is required to approximately synthesize any unitary $U(d)$ via Trotterization. Namely, using $e^{-i\hat{A}\delta t} e^{i\hat{B}\delta t} e^{i\hat{A}\delta t} e^{-i\hat{B}\delta t} = e^{[\hat{A}, \hat{B}]\delta t^2} + O(\delta t^3)$, we can engineer all possible commutators of L_x , L_z , and L_z^2 and higher order commutators. These commutators span the d -dimensional Hermitian matrices with the basis $\{\mathcal{M}_i\}_{i=1}^{d^2}$, which in turn allows to synthesize all unitary matrices. In appendix B we give an explicit construction of the enveloping algebra of L_x , L_z , and L_z^2 for $d = 3$, which allows one to generate each element of $U(3)$. As detailed in reference [52], the construction given in the appendix can be generalized to $d > 3$. In this way, the operators L_x , L_z , and L_z^2 provide universal control over each single collective spin. In the next section, we consider the entanglement of several collective spins to achieve exponential growth of the Hilbert space.

2. Unitary operations on two spins

The entanglement of different collective spins can be achieved by the exchange of delocalized phonons. The phonons are the Bogoliubov excitations of a weakly interacting condensate of atomic species B in n dimensions, where we consider $n = 1, 2$ (see figure 1). The purely phononic part of the Hamiltonian is given by

$$H_B = \sum_{\mathbf{k}} \hbar\omega_{\mathbf{k}} b_{\mathbf{k}}^{\dagger} b_{\mathbf{k}}, \quad (3)$$

where $b_{\mathbf{k}}$ is the annihilation operator of a phonon mode at wave number \mathbf{k} with components $k_i = \frac{\pi}{L} m_i$ and m_i is a positive integer. The phonon dispersion at low momenta is linear $\omega_{\mathbf{k}} \approx c|\mathbf{k}|$, where $c = \sqrt{\tilde{g}_B n_B / M_B}$ is the speed of sound determined by the interaction strength \tilde{g}_B of the B atoms with mass M_B and the density n_B , see appendix C for more details.

By immersing the collective spins into the phonon bath, we induce interactions between the phonons and the spins rooted in the contact interactions of the two atomic species A and B. The spin–phonon interaction can be described by the Hamiltonian

$$H_{AB} = \sum_{\mathbf{y}, \mathbf{k}} [\bar{g}_{\mathbf{k}}(\mathbf{y}) + \delta g_{\mathbf{k}}(\mathbf{y}) L_z(\mathbf{y})] (b_{\mathbf{k}} + \text{H.c.}), \quad (4)$$

with the explicit forms of the coupling constants $\bar{g}_{\mathbf{k}}(\mathbf{y})$ and $\delta g_{\mathbf{k}}(\mathbf{y})$. A detailed derivation of equation (4) is given in appendix D. This interaction is similar to the phonon–ion interactions in trapped ion systems [16] or photon–atom interactions [53]. The first term of equation (4) leads to a constant polaronic shift [45, 54], which can be absorbed by redefining the phonon operators. Consequently, we focus here on the second term, which can be used to generate entanglement between the spins.

Since $L_z(\mathbf{y})$ is a conserved quantity for $\Omega(\mathbf{y}) = 0$ it is possible to decouple the phonons and spins in equation (4) by shifting the phonon operators (see appendix E). Eliminating the phonons leads to an effective long-range spin–spin interaction

$$H_I = - \sum_{\mathbf{x}, \mathbf{y}} g(\mathbf{x}, \mathbf{y}) L_z(\mathbf{x}) L_z(\mathbf{y}), \quad (5)$$

where we introduced the coupling $g(\mathbf{x}, \mathbf{y})$ between the spins after a proper redefinition of $\chi(\mathbf{y})$ and $\Delta(\mathbf{y})$.

Explicitly, the coupling between the spins is given by

$$g(\mathbf{x}, \mathbf{y}) = g \sum_{\mathbf{k}} \frac{(u_{\mathbf{k}} + v_{\mathbf{k}})^2}{\hbar\omega_{\mathbf{k}}} e^{-\frac{1}{4}|\mathbf{k}|^2 \sigma_A^2} \prod_{i=1}^n \sin(k_i x_i) \sin(k_i y_i). \quad (6)$$

The overall prefactor

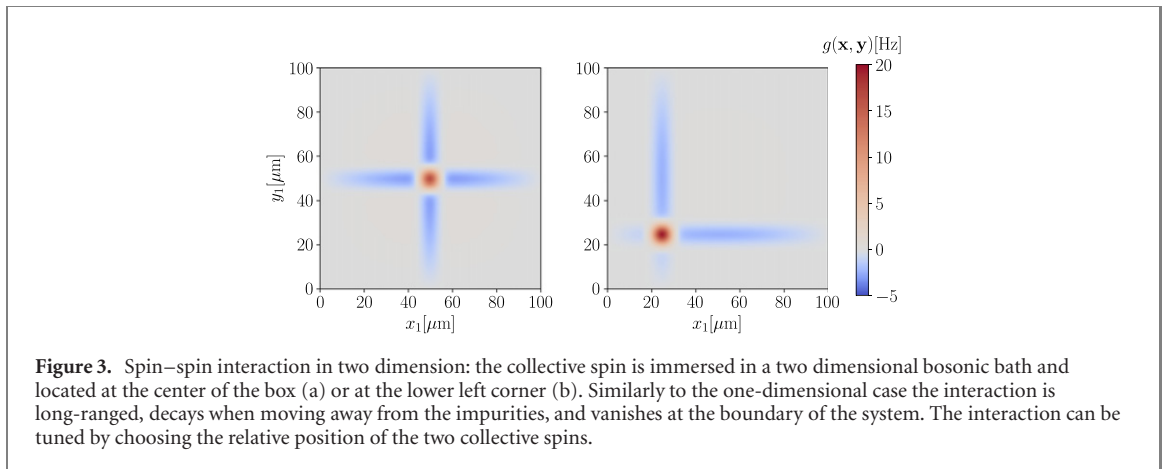
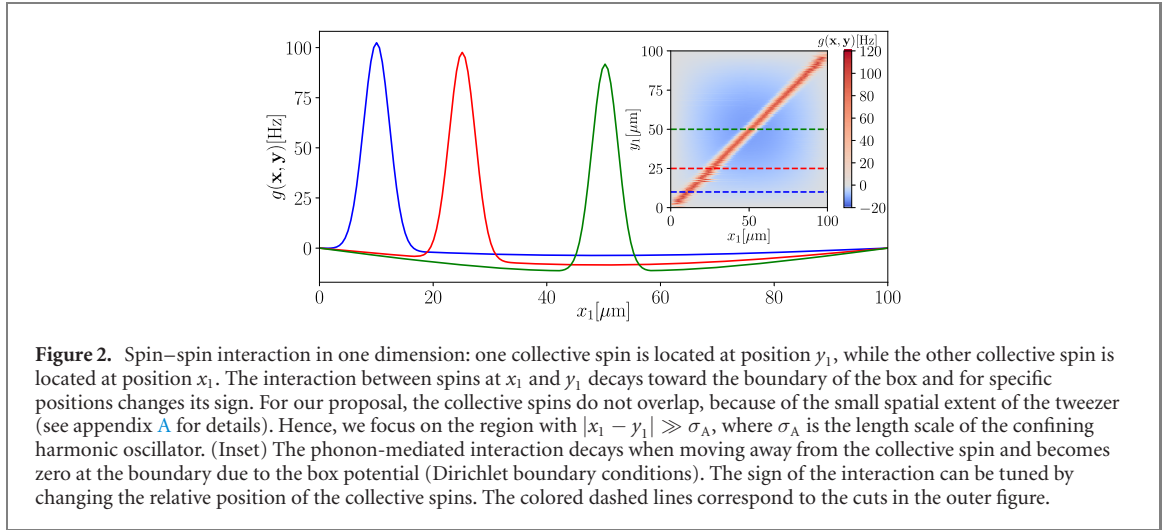
$$g = n_B (2/L)^n (\tilde{g}_{AB}^1 - \tilde{g}_{AB}^0)^2 \quad (7)$$

is determined by the inter-species interaction \tilde{g}_{AB}^0 and \tilde{g}_{AB}^1 , where the \sim indicates the renormalization according to the optical potential. Further, we introduce the Bogoliubov amplitudes $u_{\mathbf{k}}$ and $v_{\mathbf{k}}$, which are determined by performing the Bogoliubov approximation in a box potential of length L [55, 56]. We further approximate the Bogoliubov mode functions by $\sin(k_i x_i)$. The length scale σ_A is the harmonic oscillator length of the tweezer confining the A atoms, which provides a cutoff for the momentum sum in equation (6). For more details we refer to appendix D.

Performing the momentum sum numerically, the resulting interaction between two spins for one and two dimensions is illustrated in figures 2 and 3. Positioning the spins appropriately within the bath allows one to tune the strength and sign of the spin–spin interaction. The effective interaction scales as n_B independent of the dimension, as long as only the linear part of the dispersion $\omega_{\mathbf{k}}$ contributes to the sum of equation (6).

In order to entangle two specific spins, the ability to deliberately switch on and off the interactions $g(\mathbf{x}, \mathbf{y})$ is necessary. A first possibility is to physically move the optical tweezers such that there is no overlap of the collective spins with the phonons. This approach is similar to the shuttling approach in trapped ions [57].

The second approach, is similar to the optical shelving used in trapped ions [58]. The interaction between the collective spins is proportional to the scattering length difference, $g(\mathbf{x}, \mathbf{y}) \propto (\tilde{g}_{AB}^1 - \tilde{g}_{AB}^0)^2$. The first term describes the interaction strength between A atoms in $m_F = 1$ and B atoms in $m_F = 0$, while the second term describes the interaction between atoms of both species being in $m_F = 0$. To shelve spins, we can coherently transfer the $m_F = 0$ component of A atoms into the $m_F = -1$ state, while the atoms in the



$m_F = 1$ component are left unaltered. The resulting interaction is strictly zero since $g(\mathbf{x}, \mathbf{y}) \propto (\tilde{g}_{AB}^{-1} - \tilde{g}_{AB}^1)^2 = 0$.

By tuning the interaction time between the spins, using two additional single qudit gates and adding a phase allow for synthesizing a controlled-Z gate [59] between two collective spins

$$CZ(\mathbf{x}, \mathbf{y}) = e^{i\frac{2\pi}{d}L_z(\mathbf{x})L_z(\mathbf{y})} e^{i\frac{2\pi\ell}{d}L_z(\mathbf{x})} e^{i\frac{2\pi\ell}{d}L_z(\mathbf{y})} e^{i\frac{2\pi\ell^2}{d}}, \quad (8)$$

which completes the universal gate set in the multi-spin system [60, 61]. The quality of the local spin addressing and the magnetic field stability [62] will determine the fidelity of the gates.

3. State preparation and detection

A universal quantum computer requires a reliable state-preparation and readout. Using the external magnetic field one can prepare all A atoms in one hyperfine component, which corresponds to a fully polarized collective spin along the quantization axis $|\psi\rangle = |d\rangle \otimes \dots \otimes |d\rangle$. In case the particle number per site is probabilistic, one can perform post-selection to fix N_A [63–65]. If one uses instead an optical lattice to create the collective spins, one can deterministically control the atom number by preparing first a Mott-insulating state, which nowadays can be prepared with almost unit filling [26] and a subsequent merging of a fixed number of wells. For the preparation as well as for the detection one has to ensure single counting statistics per site, which can be achieved through fluorescence imaging [34].

When working in the large collective spin regime, one can efficiently prepare condensates through evaporative cooling in the optical dipole trap [66]. This results in an atomic cloud of a few hundred to thousand atoms of low entropy in each dipole trap. In case the A atoms are not in the motional ground state, one can perform Raman sideband cooling [67]. For larger collective spins, one can use homodyne detection to map out large collective spins [68].

4. Experimental characteristics

Having established all the necessary ingredients for a quantum information platform, we discuss details of a possible experimental realization as well as main sources of errors. The experiments can rely on standard experimental tools employed for cold atoms [20]. For concreteness, we focus on a mixture of ^{39}K (species A) forming the collective spins and ^{23}Na (species B) forming the phonon bath.

The collective spins can be realized through the trapping of a few atoms in optical tweezers distanced by a few micrometers and with motional ground state extension $\sigma_A \approx 100$ nm. With this confinement and working with ≈ 10 atoms per tweezer leads to three body loss between the species [69] on a time scale of ~ 1 Hz. The typical single qubit gates can then be performed with a Rabi frequency of up to a few kHz with above 99% fidelity [38]. In order to ensure the coherent evolution one has to stabilize the magnetic field, which for state of the art experiments is possible up to ~ 10 Hz. Readout reliability through fluorescence imaging differ between schemes but can reach $> 99\%$ fidelity [70–72].

Assuming a box potential for species B [55] in a tube or a slab geometry with linear dimension $L \approx 100$ μm we expect approximately 50 collective spins in a one-dimensional geometry or 2500 collective spins in a two dimensional geometry. In both cases, all-to-all coupling can be achieved through phonons of a (quasi-)condensate of approximately $N_B \approx 300 \times 10^3$ atoms for the 1D bath and $N_B \approx 3 \times 10^6$ for the 2D bath, with a transverse confinement of $\omega_\perp \approx 2\pi \times 440$ Hz, such that the condensate has a chemical potential of $\mu_B/h \approx 7.7$ kHz in 1D and $\mu_B/h \approx 1.9$ kHz in 2D [22]. This implies typical lifetimes for single atom losses that can be of several seconds up to a few minutes, setting an upper limit on the length of the quantum circuit [25].

The collective spins are coupled to the phonons through contact interaction according to the scattering length $a_0^{\text{AB}} = 756a_0$, $a_1^{\text{AB}} = 2542a_0$ and $a_2^{\text{AB}} = -437a_0$. The couplings g_{AB}^m can then be obtained by calculating the corresponding Clebsch–Gordon coefficients [73]. The speed of the entangling gates is then determined by the strength of the interaction between species A and B given by equation (6), as we illustrated in figures 2 and 3. For example, the typical gate speed of the CZ gate connecting two qudits at a distance of 5 μm can be estimated to be of the order of 50 Hz in the one-dimensional case, see figure 2. Using an optical lattice for the collective spins, 20×20 lattice sites are within the current experimental feasibilities and allow all qudits to interact with the phonons. The coupling constants and time scales of the main decoherence channels indicate, that the proposed setup is a realistic route for large-scale quantum information processing with neutral atoms, exploiting already available state-of-the-art technology.

5. Quantum error correction

QEC allows one to mitigate the effects of a noisy environment and faulty operations on the information stored in quantum states. The main idea of QEC is to embed quantum information in a Hilbert space of larger dimension, enabling a distribution of information that leads to resilience against noise. For this purpose, one can use the combined Hilbert space of multiple qubits, while an alternative approach is to use a single system that has a larger Hilbert space. A way to realize the latter goes back to a seminal work of Gottesmann, Kitaev, and Preskill (GKP) [74], which proposed encoding a qubit into a harmonic oscillator.

The *finite*-dimensional version of the GKP code encodes a qubit into a collective spin. This code is based on a set of commuting operators, the *stabilizer set*, which can be measured simultaneously. The quantum information is then encoded into the joint $(+1)$ -eigenspace of the stabilizer set. Errors acting on the encoded information may lead to a change in one or few stabilizer measurements, which helps in detecting and correcting errors.

The formalism of the finite-dimensional GKP code rests on the generalized Pauli operators X and Z defined by

$$X|j\rangle_d = |(j+1) \bmod d\rangle_d, \quad (9a)$$

$$Z|j\rangle_d = \omega^j |j\rangle_d. \quad (9b)$$

These operators obey the relation $ZX = \omega XZ$, with $\omega = \exp(2\pi i/d)$. In particular, two operators of the form $X^\alpha Z^\beta$ and $X^\gamma Z^\delta$ can commute with each other, if their exponents α, β, γ , and δ are chosen appropriately. Such operators can then be used to form the stabilizer group of a code.

To illustrate the idea behind the finite dimensional GKP code, we choose $d = 8$ corresponding to seven atoms in an optical tweezer. In order to generate the stabilizer group, we choose the operators

$$S_1 = X^4, \quad (10a)$$

$$S_2 = Z^4. \quad (10b)$$

Notice that S_1 and S_2 commute. Their joint $(+1)$ -eigenspace defines a two-dimensional subspace, which can be used to encode a logical qubit. A basis for this code space is

$$|\bar{0}\rangle = \frac{1}{\sqrt{2}}(|0\rangle_8 + |4\rangle_8), \quad (11a)$$

$$|\bar{1}\rangle = \frac{1}{\sqrt{2}}(|2\rangle_8 + |6\rangle_8). \quad (11b)$$

A state is then encoded as $|\psi_L\rangle = \alpha|\bar{0}\rangle + \beta|\bar{1}\rangle$ and one can detect all errors $X^a Z^b$ that have $|a|, |b| \leq 1$. However, from the fact that $X|\bar{0}\rangle = X^{-1}|\bar{1}\rangle$ we infer that some of these errors can only be detected, but not corrected, because the action of X and X^{-1} on the logical states cannot be distinguished. More explicitly, this can be seen from the conditions for QEC [75].

Experimentally, the two logical states $|\bar{0}\rangle, |\bar{1}\rangle$ are prepared by using a control qubit as shown in figure 4(b): the collective spin and the qubit are initially prepared in the product state $|0\rangle_2|0\rangle_8$. Applying a Hadamard gate onto the control qubit leads to $\frac{1}{\sqrt{2}}(|0\rangle_2 + |1\rangle_2)|0\rangle_8$. Next, we employ a conditional CX^4 gate defined as

$$CX^4|j\rangle_2|k\rangle_8 = (\mathbb{1} \otimes X^{4j})|j\rangle_2|k\rangle_8, \quad (12)$$

which results in $\frac{1}{\sqrt{2}}(|0\rangle_2|0\rangle_8 + |1\rangle_2|4\rangle_8)$. A second Hadamard gate on the control qubit yields

$$\frac{1}{\sqrt{2}} [|0\rangle_2|\bar{0}\rangle + |1\rangle_2(Z|\bar{0}\rangle)]. \quad (13)$$

After measuring the Z eigenvalue of the control qubit, the collective spins is projected onto either $|\bar{0}\rangle$ or $Z|\bar{0}\rangle$. In the latter case, an additional Z gate is applied. In this way, the system is deterministically prepared in $|\bar{0}\rangle$. In an experiment the circuit depicted in figure 4(b) can be realized as follows: the circuit contains Hadamard gates, which acts on a qubit, a Z -gate, which acts on a qudit, a CX^4 gate acting on a qudit and qubit, and a local readout. The Hadamard gate on the qubit is realized by performing a $\pi/2$ pulse locally. The Z -gate on the qudit is performed by changing the detuning of the microwave. The CX^4 is not a native gate described in section 2. However, since the gates generated by L_z, L_x, L_z^2 , and the CZ gate are universal, we can decompose the CX^4 gate into a judiciously chosen sequence of local gates and two-body gates. The local gates correspond to local optical control, microwave pulses, and local collision of atoms. The two-body CZ -gate corresponds to phonon entanglement, which can be switched off via optical shelving.

The encoding (11) allows one to detect certain errors affecting the logical qubit. Consider errors of the form $X^a Z^b$ acting on $|\psi_L\rangle$. From the commutation relation $S_1 X^a Z^b = \omega^{-4b} X^a Z^b S_1$ and $S_2 X^a Z^b = \omega^{4a} X^a Z^b S_2$, one obtains

$$S_1 (X^a Z^b |\psi_L\rangle) = \omega^{-4b} (X^a Z^b |\psi_L\rangle), \quad (14a)$$

$$S_2 (X^a Z^b |\psi_L\rangle) = \omega^{4a} (X^a Z^b |\psi_L\rangle). \quad (14b)$$

Thus an error may move the logical qubit out of the $(+1)$ -eigenspace of S_1 and S_2 . In particular, this happens for all non-trivial $X^a Z^b$ with $|a|, |b| \leq 1$. The circuit in figure 4(c) can then be used to detect when this happens. Likewise, it can be shown that the same circuit also detects any linear combinations of such errors.

To also correct errors, one has to use a larger collective spin. Using $d = 18$, the stabilizers $S_1 = X^6$ and $S_2 = Z^6$ yield a code with basis [74]

$$|\bar{0}\rangle = \frac{1}{\sqrt{3}} (|0\rangle_{18} + |6\rangle_{18} + |12\rangle_{18}), \quad (15a)$$

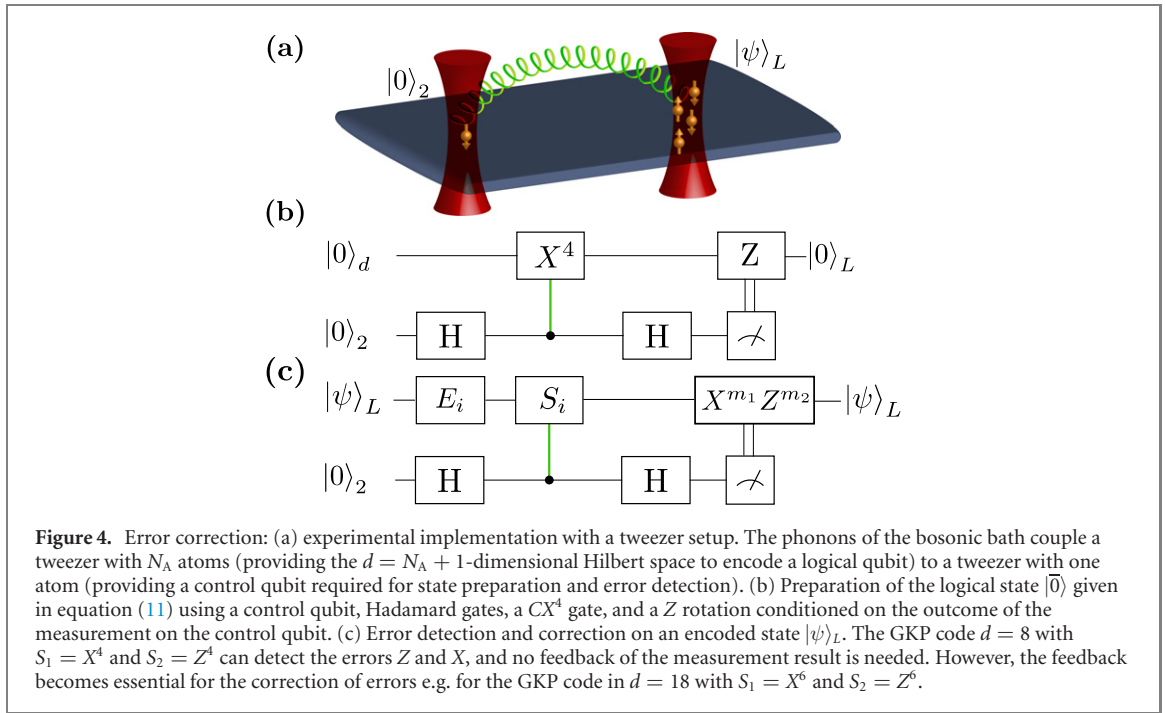
$$|\bar{1}\rangle = \frac{1}{\sqrt{3}} (|3\rangle_{18} + |9\rangle_{18} + |15\rangle_{18}). \quad (15b)$$

The circuit given in figure 4(c) can now not only detect, but also *correct* all errors $X^a Z^b$ with $|a|, |b| \leq 1$. Then, the encoded states can also be manipulated through a set of universal gates. To be specific, we return to the case of $d = 8$. The logical gates $\bar{X} = X^2$ and $\bar{Z} = Z^2$ act like the usual spin 1/2 Pauli matrices on $|\bar{0}\rangle$ and $|\bar{1}\rangle$, i.e.

$$\bar{X}|\bar{0}\rangle = |\bar{1}\rangle, \quad \bar{Z}|\bar{0}\rangle = |\bar{0}\rangle, \quad (16a)$$

$$\bar{X}|\bar{1}\rangle = |\bar{0}\rangle, \quad \bar{Z}|\bar{1}\rangle = -|\bar{1}\rangle, \quad (16b)$$

such that $\bar{X}^2 = \bar{Z}^2 = \mathbf{1}$ and $\bar{X}\bar{Z} + \bar{Z}\bar{X} = 0$.



As explained in section 1, we can implement *all* single-qubit logical gates through Trotterization, which allows to synthesize

$$\bar{\mathcal{R}}(\alpha, \beta, \gamma, \delta) = e^{i\alpha} e^{i\beta\bar{Z}} e^{i\gamma\bar{X}} e^{i\delta\bar{Z}}. \quad (17)$$

Moreover, two logical qubits can be entangled by using a logical controlled Z gate,

$$C\bar{Z}(\mathbf{x}, \mathbf{y}) = e^{i\pi\bar{Z}(\mathbf{x})\bar{Z}(\mathbf{y})}, \quad (18)$$

which can be also synthesized via Trotterization using the gates generated by L_x , L_z and L_z^2 , and the entangling gate $CZ(\mathbf{x}, \mathbf{y})$ given in equation (8). Together, the operations $\bar{\mathcal{R}}(\alpha, \beta, \gamma, \delta)$ and $C\bar{Z}$ then generate a universal set of logical gates [60].

In summary, we have constructed an explicit example of a quantum error-detecting code for $d = 8$, described the experimental preparation of its logical states, and provided a universal gate set to manipulate the stored quantum information. The presented formalism will also work in larger dimensions, allowing for the detection and correction of a larger set of errors [74]. The here proposed platform with a suitable quantum error-correcting scheme, such as finite GKP codes, may allow one to go beyond the abilities of noisy intermediate-scale quantum (NISQ) technologies.

6. Conclusion and outlook

In this work, we have proposed a mixture of two ultracold atomic species as a platform for universal quantum computation. Our proposed implementation uses long-range entangling gates and, in addition, allows for the realization of QEC. The idea of using phonon mediated interactions for quantum information processing is also discussed in the solid state context and made substantial progress [76, 77]. The presented spin–phonon system is not only useful for the processing of quantum information but is also interesting from a quantum many-body perspective. The many body systems realized by our platform is similar to gauge theories coupled to a Higgs field [78–80] and hence is a promising candidate for the investigation of topological matter. Further, the spin–phonon system proposed here may give access to the physics of the Peierls transition [81], the Jahn–Teller effect [82] in a many-body context as well as the study of frustrated spin models [83]. The versatility of this platform also makes it an ideal candidate for a fully programmable quantum simulation, whose large potential has been demonstrated in Rydberg and trapped ion systems [4, 5, 84, 85]. For example, atomic mixtures have been proposed for the quantum simulation of quantum chemistry problems [86].

In future work, the building blocks of our proposed platform could be exchanged ad libitum exploiting the versatility of atomic, molecular, and atomic physics. The basic unit of information can be stored, e.g. with spinful fermions in an optical tweezer [71] or higher dimensional spins [38, 87, 88]. The entanglement bus may be substituted by more complex many-body excitations like magnons or rotons [89, 90]. This

exchange of the basic unit of information and the entanglement mechanism has the potential to lead to new implementations of quantum algorithms and QEC schemes, see for example [91–94]. Thus, ultracold atom mixtures present a promising platform to implement fault-tolerant quantum computation in a scalable platform, paving a way beyond the abilities of NISQ technology.

Acknowledgments

The authors are grateful for fruitful discussions with J Eisert, M Gaerttner, T Gasenzer, M Gluza, S Jochim, M Oberthaler, A P Orioli, P Preiss, H Strobel and all the members of the SynQs seminar. ICFO group acknowledges support from ERC AdG NOQIA, State Research Agency AEI (Severo Ochoa Center of Excellence CEX2019-000910-S, Plan National FIDEUA PID2019-106901GB-I00/10.13039/501100011033, FPI, QUANTERA MAQS PCI2019-111828-2/ 10.13039/501100011033), Fundació Privada Cellex, Fundació Mir-Puig, Generalitat de Catalunya (AGAUR Grant No. 2017 SGR 1341, CERCA program, QuantumCAT / U16-011424, co-funded by ERDF Operational Program of Catalonia 2014-2020), EU Horizon 2020 FET-OPEN OPTOLogic (Grant No 899794), and the National Science Centre, Poland (Symfonia Grant No. 2016/20/W/ST4/00314), Marie Skłodowska-Curie grant STREDCH No.101029393, La Caixa Junior Leaders fellowships (ID100010434), and EU Horizon 2020 under Marie Skłodowska-Curie Grant Agreement No. 847648 (LCF/BQ/PI19/11690013, LCF/BQ/PI20/11760031, LCF/BQ/PR20/11770012). FH acknowledges the Government of Spain (FIS2020-TRANQI and Severo Ochoa CEX2019-000910-S), Fundació Cellex, Fundació Mir-Puig, Generalitat de Catalunya (CERCA, AGAUR SGR 1381), and the Foundation for Polish Science through TEAM-NET (POIR.04.04.00-00-17C1/18-00). PH acknowledges support by Q@TN—Quantum Science and Technologies at Trento, the Provincia Autonoma di Trento, and the ERC Starting Grant StrEnQTh (Project-ID 804305). This work is part of and supported by the DFG Collaborative Research Center ‘SFB 1225 (ISOQUANT)’. FJ acknowledges the DFG support through the Project FOR 2724, the Emmy-Noether Grant (Project-ID 377616843) and support by the Bundesministerium für Wirtschaft und Energie through the project ‘EnerQuant’ (Project-ID 03EI1025C).

Data availability statement

The data that support the findings of this study are available upon reasonable request from the authors.

Appendix A. Collective spin Hamiltonian

The type A atoms are placed in an external magnetic field, which allows to prepare the atoms in magnetic substates $m \in \{0, 1\}$. Further, the atoms of type A are localized at specific sites via optical potentials (see figure 1). The single particle physics is described by the Hamiltonian

$$H_A^m(\mathbf{x}) = -\frac{\hbar^2 \nabla_{\mathbf{x}}^2}{2M_A} + V_A(\mathbf{x}) + E_m^m(B), \quad (\text{A1})$$

where M_A is the mass of the atoms and $V_A(\mathbf{x})$ is the optical potential confining the atoms. The energy shift $E_m^m(B)$ determined by the magnetic field B is given by

$$E_m^m(B) = p_m(B)m + q_m(B)m^2, \quad (\text{A2})$$

where $p_m(B)$ parametrizes the linear Zeeman shift and $q_m(B)$ the quadratic Zeeman shift. The field operators $A_m(\mathbf{x})$ and $A_m^\dagger(\mathbf{x})$ annihilate and create a particle at position $\mathbf{x} = (x_1, \dots, x_d)^T$ respectively and fulfill canonical commutation relations. The many-body Hamiltonian is given by

$$H_A = \sum_m \int_{\mathbf{x}} A_m^\dagger(\mathbf{x}) H_A^m(\mathbf{x}) A_m(\mathbf{x}) + \sum_{m,n} \int_{\mathbf{x}} \frac{g_{\Lambda}^{mn}}{2} A_m^\dagger(\mathbf{x}) A_n^\dagger(\mathbf{x}) A_n(\mathbf{x}) A_m(\mathbf{x}). \quad (\text{A3})$$

The atoms are localized at different sites \mathbf{y} , which allows one to expand the field operators as

$$A_m(\mathbf{x}) = \sum_{\mathbf{y}} \varphi_{\Lambda}(\mathbf{x} - \mathbf{y}) a_m(\mathbf{y}) \quad (\text{A4})$$

with a wave function φ_A localized at $\mathbf{0}$ and which does not depend on the magnetic substate. Inserting the expansion (A4) into H_A and neglecting the tunneling terms, we obtain the Hamiltonian

$$H_A = \frac{1}{2} \sum_{m,n,y} \tilde{g}_A^{mn} a_m^\dagger(\mathbf{y}) a_n^\dagger(\mathbf{y}) a_m(\mathbf{y}) a_n(\mathbf{y}) \quad (\text{A5})$$

with the overlap integrals

$$\tilde{g}_A^{mn} = g_A^{mn} \int_{\mathbf{x}} |\varphi_A(\mathbf{x} - \mathbf{y})|^4. \quad (\text{A6})$$

To be explicit, we approximate $\varphi_A(\mathbf{x})$ by the ground state wavefunction of an isotropic harmonic oscillator $\varphi_A(\mathbf{x}) = \varphi_A(x_1)\varphi_A(x_2)\varphi_A(x_3)$ with

$$\varphi_A(x_i) = (\sqrt{\pi}\sigma_A)^{-1/2} e^{-\frac{1}{2}\left(\frac{x_i}{\sigma_A}\right)^2} \quad (\text{A7})$$

with the characteristic length σ_A . Calculating the overlap integral leads to the dimensional reduced coupling constant

$$\tilde{g}_A^{mn} = (2\pi)^{-3/2} (g_A^{mn}/\sigma_A^3). \quad (\text{A8})$$

Inserting the Schwinger representation of the angular momentum into equation (A5) leads to equation (2) with the coupling constants

$$\chi = \frac{1}{2} (\tilde{g}_A^{00} + \tilde{g}_A^{11} - 2\tilde{g}_A^{10}), \quad (\text{A9a})$$

$$\Delta = \frac{1}{2} (N_A - 1) (\tilde{g}_A^{11} - \tilde{g}_A^{00}) + E_A^1 - E_A^0, \quad (\text{A9b})$$

where N_A is the particle number on each site.

Appendix B. Enveloping algebra of $U(3)$

In this appendix, we demonstrate for $\ell = 1$ that L_z , L_x , and L_z^2 are sufficient to generate all $U(3)$ matrices. We use the spin matrices

$$L_x = \frac{1}{\sqrt{2}} \begin{pmatrix} 0 & 1 & 0 \\ 1 & 0 & 1 \\ 0 & 1 & 0 \end{pmatrix}, \quad L_y = \frac{1}{\sqrt{2}i} \begin{pmatrix} 0 & 1 & 0 \\ -1 & 0 & 1 \\ 0 & -1 & 0 \end{pmatrix}, \quad L_z = \begin{pmatrix} 1 & 0 & 0 \\ 0 & 0 & 0 \\ 0 & 0 & -1 \end{pmatrix}.$$

Consider the following matrices generated by commutators of L_x , L_z , and L_z^2

$$\begin{aligned} \mathcal{M}_1 &= L_x, & \mathcal{M}_2 &= L_z, & \mathcal{M}_3 &= L_z^2, \\ \mathcal{M}_4 &= i[\mathcal{M}_1, \mathcal{M}_2], & \mathcal{M}_5 &= i[\mathcal{M}_3, \mathcal{M}_1], & \mathcal{M}_6 &= i[\mathcal{M}_3, \mathcal{M}_4], \\ \mathcal{M}_7 &= i[\mathcal{M}_5, \mathcal{M}_1], & \mathcal{M}_8 &= i[\mathcal{M}_5, \mathcal{M}_4], & \mathcal{M}_9 &= i[\mathcal{M}_6, \mathcal{M}_4]. \end{aligned} \quad (\text{B1})$$

These commutators form a basis for the Lie algebra of $U(3)$. This can be explicitly checked by constructing a change of basis from the $\{\mathcal{M}_i\}_{i=1}^9$ to the canonical basis of Hermitian matrices $\{M_i\}_{i=1}^9$ given by

$$\begin{aligned} M_1 &= \begin{pmatrix} 1 & 0 & 0 \\ 0 & 0 & 0 \\ 0 & 0 & 0 \end{pmatrix}, & M_2 &= \begin{pmatrix} 0 & 0 & 0 \\ 0 & 1 & 0 \\ 0 & 0 & 0 \end{pmatrix}, & M_3 &= \begin{pmatrix} 0 & 0 & 0 \\ 0 & 0 & 0 \\ 0 & 0 & 1 \end{pmatrix}, \\ M_4 &= \begin{pmatrix} 0 & 1 & 0 \\ 1 & 0 & 0 \\ 0 & 0 & 0 \end{pmatrix}, & M_5 &= \begin{pmatrix} 0 & 0 & 1 \\ 0 & 0 & 0 \\ 1 & 0 & 0 \end{pmatrix}, & M_6 &= \begin{pmatrix} 0 & 0 & 0 \\ 0 & 0 & 1 \\ 0 & 1 & 0 \end{pmatrix}, \\ M_7 &= \begin{pmatrix} 0 & i & 0 \\ -i & 0 & 0 \\ 0 & 0 & 0 \end{pmatrix}, & M_8 &= \begin{pmatrix} 0 & 0 & i \\ 0 & 0 & 0 \\ -i & 0 & 0 \end{pmatrix}, & M_9 &= \begin{pmatrix} 0 & 0 & 0 \\ 0 & 0 & i \\ 0 & -i & 0 \end{pmatrix}. \end{aligned} \quad (\text{B2})$$

Appendix C. Phonon Hamiltonian

The Hamiltonian involving only the atomic species B is given by

$$H_B = \int_{\mathbf{x}} B^\dagger(\mathbf{x}) H_B^0(\mathbf{x}) B(\mathbf{x}) + \frac{g_B}{2} \int_{\mathbf{x}} B^\dagger(\mathbf{x}) B^\dagger(\mathbf{x}) B(\mathbf{x}) B(\mathbf{x}) \quad (C1)$$

with

$$H_B^0(\mathbf{x}) = -\frac{\hbar^2 \nabla_{\mathbf{x}}^2}{2M_B} + V_B(\mathbf{x}). \quad (C2)$$

In order to create a one- or two-dimensional phononic bath we apply the following harmonic and isotropic confinement

$$V_B(\mathbf{x}) = \frac{1}{2} M_B \omega_B^2 \sum_{i=n+1}^d x_i^2. \quad (C3)$$

For sufficiently low temperatures, the transversal degrees of freedom will not be excited, which will confine the particles effectively to one ($n = 1$) or two ($n = 2$) dimensions respectively. This freezing out of the transversal directions allows one to write the field operator as

$$B(\mathbf{x}) = B(x_1, \dots, x_n) \varphi_B(x_{n+1}, \dots, x_d) \quad (C4)$$

with the transversal wave function $\varphi_B(x_{n+1}, \dots, x_d)$ and $B(x_1, \dots, x_n)$ the annihilation operator in n dimensions, and in the following we will use $\tilde{\mathbf{x}} = (x_1, \dots, x_n)^T$. The stationary Gross–Pitaevskii equation is given by

$$0 = \left[-\frac{\hbar^2 \nabla_{\tilde{\mathbf{x}}}^2}{2M_B} - \mu_B + \tilde{g}_B |\phi_B(\tilde{\mathbf{x}})|^2 \right] \phi_B(\tilde{\mathbf{x}}) \quad (C5)$$

with the condensate $\phi_B(\tilde{\mathbf{x}})$ fulfilling the Dirichlet boundary conditions $\phi_B(\tilde{\mathbf{x}}) = 0$ for $\tilde{\mathbf{x}} \in \partial D$ with $D = [0, L]^n$ and chemical potential μ_B . The coupling constant is given by

$$\tilde{g}_B = g_B \int_{x_{n+1}, \dots, x_d} |\varphi_B(x_{n+1}, \dots, x_d)|^4, \quad (C6)$$

which becomes $\tilde{g}_B = (\sqrt{2\pi}\sigma_B)^{-(d-n)} g_B$ for harmonic confinement. The bulk solution of the Gross–Pitaevskii equation can be approximated by the homogeneous function

$$\phi_B(\tilde{\mathbf{x}}) \approx \sqrt{\frac{\mu_B}{\tilde{g}_B}} \quad (C7)$$

leading to the density $n_B = \frac{\mu_B}{g_B}$. In order to study the excitations of the bulk solution, we perform the Bogoliubov approximation

$$B(\tilde{\mathbf{x}}) = \phi_B(\tilde{\mathbf{x}}) + \delta B(\tilde{\mathbf{x}}), \quad (C8)$$

where δB and δB^\dagger fulfill canonical commutation relations. The Bogoliubov Hamiltonian approximation of H_B is given by

$$H_B = \int_D \left[\frac{\hbar^2}{2M_B} |\nabla_{\tilde{\mathbf{x}}} \delta B|^2 - \mu_B |\delta B|^2 + 2\tilde{g}_B |\delta B|^2 |\phi_B|^2 + \frac{\tilde{g}_B}{2} [(\delta B^\dagger)^2 (\phi_B)^2 + (\delta B)^2 (\phi_B^*)^2] \right]. \quad (C9)$$

The equations of motions can be solved by using the mode expansion

$$\delta B(\tilde{\mathbf{x}}, t) = \sum_{\mathbf{k}} \left[b_{\mathbf{k}} u_{\mathbf{k}}(\tilde{\mathbf{x}}) e^{-i\omega_{\mathbf{k}} t} + b_{\mathbf{k}}^\dagger v_{\mathbf{k}}^*(\tilde{\mathbf{x}}) e^{i\omega_{\mathbf{k}} t} \right], \quad (C10)$$

where the sum does not include the condensate mode [95]. This expansion leads to the following generalized eigenvalue problem

$$\omega_{\mathbf{k}} \begin{pmatrix} 1 & 0 \\ 0 & -1 \end{pmatrix} \begin{pmatrix} u_{\mathbf{k}} \\ v_{\mathbf{k}} \end{pmatrix} = \begin{pmatrix} h(\tilde{\mathbf{x}}) & \tilde{g}_B (\phi_B)^2 \\ \tilde{g}_B (\phi_B^*)^2 & h(\tilde{\mathbf{x}}) \end{pmatrix} \begin{pmatrix} u_{\mathbf{k}} \\ v_{\mathbf{k}} \end{pmatrix}, \quad (C11)$$

with

$$h(\tilde{\mathbf{x}}) = -\frac{\hbar^2 \nabla_{\tilde{\mathbf{x}}}^2}{2M_B} - \mu_B + 2\tilde{g}_B |\phi_B(\tilde{\mathbf{x}})|^2. \quad (C12)$$

Solving this generalized eigenvalue problem will lead to the orthonormalization condition

$$\int_D [u_{\mathbf{k}}^*(\tilde{\mathbf{x}})u_{\mathbf{k}'}(\tilde{\mathbf{x}}) - v_{\mathbf{k}}^*(\tilde{\mathbf{x}})v_{\mathbf{k}'}(\tilde{\mathbf{x}})] = \delta_{\mathbf{k},\mathbf{k}'}. \quad (\text{C13})$$

Since the background-field is approximately constant and because of the Dirichlet boundary conditions, we make the ansatz

$$u_{\mathbf{k}}(\tilde{\mathbf{x}}) = u_{\mathbf{k}} \left(\frac{2}{L} \right)^{n/2} \prod_{i=1}^n \sin(k_i x_i), \quad (\text{C14a})$$

$$v_{\mathbf{k}}(\tilde{\mathbf{x}}) = v_{\mathbf{k}} \left(\frac{2}{L} \right)^{n/2} \prod_{i=1}^n \sin(k_i x_i), \quad (\text{C14b})$$

with $k_i = \frac{n_i \pi}{L}$ and $n_i \geq 2$ and the amplitudes are given by

$$u_{\mathbf{k}}^2 = \frac{1}{2} \left(\frac{\varepsilon_{\mathbf{k}}}{\omega_{\mathbf{k}}} + 1 \right), \quad (\text{C15a})$$

$$v_{\mathbf{k}}^2 = \frac{1}{2} \left(\frac{\varepsilon_{\mathbf{k}}}{\omega_{\mathbf{k}}} - 1 \right), \quad (\text{C15b})$$

with $\varepsilon_{\mathbf{k}} = (\hbar^2 \mathbf{k}^2)/(2M_B) + \tilde{g}_B |\phi_B|^2$. The Bogoliubov eigenfrequencies of the excitations are given by

$$\hbar\omega_{\mathbf{k}} = \sqrt{\frac{\hbar^2 \mathbf{k}^2}{2M_B} \left(\frac{\hbar^2 \mathbf{k}^2}{2M_B} + 2\mu_B \right)}. \quad (\text{C16})$$

The Dirichlet boundary conditions can be achieved by box potentials, which lead to a homogeneous Bose–Einstein condensate.

Appendix D. Spin–phonon interaction

In order to derive the interaction between the phonons and the collective spins, we start from Hamiltonian modeling the interaction between the A and B atoms

$$H_{AB} = \sum_m \int_{\mathbf{x}} \frac{\tilde{g}_{AB}^m}{2} A_m^\dagger(\mathbf{x}) A_m(\mathbf{x}) B^\dagger(\mathbf{x}) B(\mathbf{x}). \quad (\text{D1})$$

After reducing the dimension and considering the tight confinement of the spins, i.e. equations (C4) and (A4), we obtain the Hamiltonian

$$H_{AB} = \sum_{m,\mathbf{y}} \frac{\tilde{g}_{AB}^m}{2} a_m^\dagger(\mathbf{y}) a_m(\mathbf{y}) \int_D |\varphi_A(x_1 - y_1) \dots \varphi_A(x_n - y_n)|^2 B^\dagger(\tilde{\mathbf{x}}) B(\tilde{\mathbf{x}}), \quad (\text{D2})$$

where we neglected hopping of the A atoms and introduced the coupling constant

$$\tilde{g}_{AB}^m = g_{AB}^m \int_{x_{n+1}, \dots, x_d} |\varphi_B(x_{n+1}) \dots \varphi_B(x_d)|^2 |\varphi_A(x_{n+1} - y_{n+1}) \dots \varphi_A(x_d - y_d)|^2, \quad (\text{D3})$$

which can be written as

$$\tilde{g}_{AB}^m = g_{AB}^m [\pi(\sigma_A^2 + \sigma_B^2)]^{-(d-n)/2} \quad (\text{D4})$$

for harmonic confinement of the A and B atoms with harmonic oscillator length scale σ_A and σ_B respectively. Expanding the field operator B in fluctuations as in equation (C8) and neglecting terms of order $\mathcal{O}(\delta B^2)$ one obtains a Hamiltonian

$$H_{AB} = H_{AB}^{(0)} + H_{AB}^{(1)}, \quad (\text{D5})$$

where $H_{AB}^{(0)}$ is independent of the fluctuations and $H_{AB}^{(1)}$ is linear in the fluctuations. The first contribution is given by

$$H_{AB}^{(0)} = \sum_{m,\mathbf{y}} \Delta_m a_m^\dagger(\mathbf{y}) a_m(\mathbf{y}), \quad (\text{D6})$$

with the coupling constant

$$\Delta_m = \frac{1}{2} \tilde{g}_{AB}^m n_B \int_D |\varphi_A(x_1 - y_1) \dots \varphi_A(x_n - y_n)|^2, \quad (\text{D7})$$

and since the harmonic oscillator wave functions are normalized we obtain

$$\Delta_m = \frac{1}{2} \tilde{g}_{AB}^m n_B. \quad (\text{D8})$$

The contribution linear in the fluctuations is given by

$$H_{AB} = \frac{\sqrt{n_B}}{2} \sum_{m,\mathbf{y}} \tilde{g}_{AB}^m a_m^\dagger(\mathbf{y}) a_m(\mathbf{y}) \int_D [\delta B(\tilde{\mathbf{x}}) + \text{H.c.}] |\varphi_A(x_1 - y_1) \dots \varphi_A(x_n - y_n)|^2. \quad (\text{D9})$$

Inserting the mode expansion (C10) into $H_{AB}^{(1)}$ we obtain

$$H_{AB}^{(1)} = \sum_{m,\mathbf{y},\mathbf{k}} \tilde{g}_{AB,\mathbf{k}}^m a_m^\dagger(\mathbf{y}) a_m(\mathbf{y}) [b_{\mathbf{k}} + \text{H.c.}], \quad (\text{D10})$$

where we introduced the coupling constant

$$\tilde{g}_{AB,\mathbf{k}}^m(\mathbf{y}) = \frac{\sqrt{n_B}}{2} \tilde{g}_{AB}^m \int_D |\varphi_A(x_1 - y_1) \dots \varphi_A(x_n - y_n)|^2 [u_{\mathbf{k}}(\tilde{\mathbf{x}}) + v_{\mathbf{k}}(\tilde{\mathbf{x}})]. \quad (\text{D11})$$

Inserting (C14) and (A7) we obtain for $L \gg \sigma_B$ approximately

$$\begin{aligned} \tilde{g}_{AB,\mathbf{k}}^m(\mathbf{y}) &= \tilde{g}_{AB}^m \sqrt{n_B} \left(\frac{2}{L}\right)^{n/2} (u_{\mathbf{k}} + v_{\mathbf{k}}) e^{-\frac{1}{4}(\mathbf{k}\alpha)^2} \\ &\times \prod_{i=1}^n \sin(k_i y_i). \end{aligned} \quad (\text{D12})$$

Using the Schwinger representation (see equation (1)), we obtain the interaction between the spins and the phonons

$$H_{AB}^{(1)} = \sum_{m,\mathbf{y},\mathbf{k}} \tilde{g}_{AB,\mathbf{k}}^m(\mathbf{y}) [L(\mathbf{y}) - (-1)^m L_z(\mathbf{y})] (b_{\mathbf{k}} + \text{H.c.}), \quad (\text{D13})$$

with $L(\mathbf{y})$ being the length of the angular momentum on site \mathbf{y} . Reshuffling terms leads to equation (4) with the coupling constants

$$\bar{g}_{\mathbf{k}}(\mathbf{y}) = L(\mathbf{y}) [\tilde{g}_{AB,\mathbf{k}}^0(\mathbf{y}) + \tilde{g}_{AB,\mathbf{k}}^1(\mathbf{y})], \quad (\text{D14a})$$

$$\delta g_{\mathbf{k}}(\mathbf{y}) = \tilde{g}_{AB,\mathbf{k}}^1(\mathbf{y}) - \tilde{g}_{AB,\mathbf{k}}^0(\mathbf{y}). \quad (\text{D14b})$$

Appendix E. Eliminating phonons

Assuming $\Omega(\mathbf{y}) = 0$ and given the approximations of appendices A, C and D the Hamiltonian $H = H_A + H_B + H_{AB}$ is diagonal in L_z , which allows us to treat phonons and spins separately. The Heisenberg equation of motion for the phonons is

$$i\hbar \partial_t b_{\mathbf{k}} = \hbar \omega_{\mathbf{k}} b_{\mathbf{k}} + \delta b_{\mathbf{k}} \quad (\text{E1})$$

of $b_{\mathbf{k}}$ operators, where we introduced the abbreviation

$$\delta b_{\mathbf{k}} = \sum_{\mathbf{y}} [\bar{g}_{\mathbf{k}}(\mathbf{y}) L(\mathbf{y}) + \delta g_{\mathbf{k}}(\mathbf{y}) L_z(\mathbf{y})]. \quad (\text{E2})$$

We define a shifted annihilation operator as

$$\beta_{\mathbf{k}} = b_{\mathbf{k}} + (\hbar\omega_{\mathbf{k}})^{-1}\delta b_{\mathbf{k}}. \quad (\text{E3})$$

Inserting the shifted operator in the Hamiltonian equation (4) leads to a spin–spin interaction










$$H_I = -\sum_{\mathbf{x},\mathbf{y}} g(\mathbf{x},\mathbf{y})L_z(\mathbf{x})L_z(\mathbf{y}) \quad (\text{E4})$$

with

$$g(\mathbf{x},\mathbf{y}) = \sum_{\mathbf{k}} (\hbar\omega_{\mathbf{k}})^{-1}\delta g_{\mathbf{k}}(\mathbf{x})\delta g_{\mathbf{k}}(\mathbf{y}). \quad (\text{E5})$$

Inserting the explicit expression for $\delta g_{\mathbf{k}}(\mathbf{x})$, we obtain equation (6).

ORCID iDs

Valentin Kasper  <https://orcid.org/0000-0001-7687-663X>
 Daniel González-Cuadra  <https://orcid.org/0000-0001-7804-7333>
 Apoorva Hegde  <https://orcid.org/0000-0001-9996-9126>
 Andy Xia  <https://orcid.org/0000-0002-7486-1589>
 Alexandre Dauphin  <https://orcid.org/0000-0003-4996-2561>
 Felix Huber  <https://orcid.org/0000-0002-3856-4018>
 Maciej Lewenstein  <https://orcid.org/0000-0002-0210-7800>
 Fred Jendrzejewski  <https://orcid.org/0000-0003-1488-7901>
 Philipp Hauke  <https://orcid.org/0000-0002-0414-1754>

References

- [1] Acin A *et al* 2018 *New J. Phys.* **20** 080201
- [2] Horodecki R, Horodecki P, Horodecki M and Horodecki K 2009 *Rev. Mod. Phys.* **81** 865
- [3] Terhal B M 2015 *Rev. Mod. Phys.* **87** 307
- [4] Bernien H *et al* 2017 *Nature* **551** 579
- [5] Zhang J, Pagano G, Hess P W, Kyprianidis A, Becker P, Kaplan H, Gorshkov A V, Gong Z-X and Monroe C 2017 *Nature* **551** 601
- [6] Arute F *et al* 2019 *Nature* **574** 505
- [7] Nigg D, Müller M, Martinez E A, Schindler P, Hennrich M, Monz T, Martin-Delgado M A and Blatt R 2014 *Science* **345** 302
- [8] Flühmann C, Nguyen T L, Marinelli M, Negnevitsky V, Mehta K and Home J P 2019 *Nature* **566** 513
- [9] Campagne-Ibarcq P *et al* 2020 *Nature* **584** 368
- [10] Andersen C K, Remm A, Lazar S, Krinner S, Lacroix N, Norris G J, Gabureac M, Eichler C and Wallraff A 2020 *Nat. Phys.* **16** 875
- [11] Vandersypen L M K, Steffen M, Breyta G, Yannoni C S, Sherwood M H and Chuang I L 2001 *Nature* **414** 883
- [12] Doherty M W, Manson N B, Delaney P, Jelezko F, Wrachtrup J and Hollenberg L C L 2013 *Phys. Rep.* **528** 1
- [13] Knill E, Laflamme R and Milburn G J 2001 *Nature* **409** 46
- [14] Watson T F *et al* 2018 *Nature* **555** 633
- [15] Krantz P, Kjaergaard M, Yan F, Orlando T P, Gustavsson S and Oliver W D 2019 *Appl. Phys. Rev.* **6** 021318
- [16] Bruzewicz C D, Chiaverini J, McConnell R and Sage J M 2019 *Appl. Phys. Rev.* **6** 021314
- [17] Nigmatullin R, Ballance C J, de Beaudrap N and Benjamin S C 2016 *New J. Phys.* **18** 103028
- [18] Pagano G *et al* 2018 *Quantum Sci. Technol.* **4** 014004
- [19] Campbell E T, Terhal B M and Vuillot C 2017 *Nature* **549** 172
- [20] Bloch I, Dalibard J and Zwerger W 2008 *Rev. Mod. Phys.* **80** 885
- [21] Cirac J I and Zoller P 2012 *Nat. Phys.* **8** 264
- [22] Lewenstein M, Sanpera A and Ahufinger V 2012 *Ultracold Atoms in Optical Lattices: Simulating Quantum Many-Body Systems* (Oxford: Oxford University Press)
- [23] Görg F, Sandholzer K, Minguzzi J, Desbuquois R, Messer M and Esslinger T 2019 *Nat. Phys.* **15** 1161
- [24] Schweizer C, Grusdt F, Berngruber M, Barbiero L, Demler E, Goldman N, Bloch I and Aidelsburger M 2019 *Nat. Phys.* **15** 1168
- [25] Mil A, Zache T V, Hegde A, Xia A, Bhatt R P, Oberthaler M K, Hauke P, Berges J and Jendrzejewski F 2020 *Science* **367** 1128
- [26] Yang B, Sun H, Ott R, Wang H-Y, Zache T V, Halimeh J C, Yuan Z-S, Hauke P and Pan J-W 2020 *Nature* **587** 392
- [27] Bañuls M C *et al* 2020 *Eur. Phys. J. D* **74** 165
- [28] Jaksch D 2004 *Contemp. Phys.* **45** 367
- [29] Brickman Soderberg K-A, Gemelke N and Chin C 2009 *New J. Phys.* **11** 055022
- [30] Saffman M, Walker T G and Mølmer K 2010 *Rev. Mod. Phys.* **82** 2313
- [31] Omran A *et al* 2019 *Science* **365** 570
- [32] Yang B, Sun H, Huang C-J, Wang H-Y, Deng Y, Dai H-N, Yuan Z-S and Pan J-W 2020 *Science* **369** 550
- [33] Madjarov I S *et al* 2020 *Nat. Phys.* **16** 857
- [34] Strobel H, Muessel W, Linnemann D, Zibold T, Hume D B, Pezzè L, Smerzi A and Oberthaler M K 2014 *Science* **345** 424
- [35] Lücke B, Peise J, Vitagliano G, Arlt J, Santos L, Tóth G and Klempt C 2014 *Phys. Rev. Lett.* **112** 155304
- [36] Bookjans E M, Vinit A and Raman C 2011 *Phys. Rev. Lett.* **107** 195306
- [37] Pezzè L, Smerzi A, Oberthaler M K, Schmied R and Treutlein P 2018 *Rev. Mod. Phys.* **90** 035005
- [38] Stamper-Kurn D M and Ueda M 2013 *Rev. Mod. Phys.* **85** 1191
- [39] Kunkel P, Prüfer M, Strobel H, Linnemann D, Frölian A, Gasenzer T, Gärttner M and Oberthaler M K 2018 *Science* **360** 413

- [40] Klein A and Fleischhauer M 2005 *Phys. Rev. A* **71** 33605
- [41] Klein A, Bruderer M, Clark S R and Jaksch D 2007 *New J. Phys.* **9** 411
- [42] Diehl S, Micheli A, Kantian A, Kraus B, Büchler H P and Zoller P 2008 *Nat. Phys.* **4** 878
- [43] Ramos T, Pichler H, Daley A J and Zoller P 2014 *Phys. Rev. Lett.* **113** 237203
- [44] Scelle R, Rentrop T, Trautmann A, Schuster T and Oberthaler M K 2013 *Phys. Rev. Lett.* **111** 070401
- [45] Rentrop T, Trautmann A, Olivares F A, Jendrzejewski F, Komnik A and Oberthaler M K 2016 *Phys. Rev. X* **6** 041041
- [46] DiVincenzo D P 2000 *Fortschr. Phys.* **48** 771
- [47] If not stated otherwise we will assume the same number of atoms at all site y , whereas different atom number per sites are in principle possible.
- [48] Weitenberg C, Endres M, Sherson J F, Cheneau M, Schauß P, Fukuhara T, Bloch I and Kuhr S 2011 *Nature* **471** 319
- [49] Farolfi A, Zenesini A, Cominotti R, Trypogeorgos D, Recati A, Lamporessi G and Ferrari G 2021 *Phys. Rev. A* **104** 023326
- [50] Wineland D J et al 2003 *Phil. Trans. R. Soc. A* **361** 1349
- [51] Nielsen M A and Chuang I L 2013 *Quantum Computation and Quantum Information* (Cambridge: Cambridge University Press)
- [52] Giorda P, Zanardi P and Lloyd S 2003 *Phys. Rev. A* **68** 062320
- [53] Chang D E, Douglas J S, González-Tudela A, Hung C-L and Kimble H J 2018 *Rev. Mod. Phys.* **90** 31002
- [54] Grusdt F and Demler E 2015 arXiv:1510.04934
- [55] Lopes R, Eigen C, Navon N, Clément D, Smith R P and Hadzibabic Z 2017 *Phys. Rev. Lett.* **119** 190404
- [56] Rauer B, Erne S, Schweigler T, Cataldini F, Tajik M and Schmiedmayer J 2018 *Science* **360** 307
- [57] Kaushal V et al 2020 *AVS Quantum Sci.* **2** 014101
- [58] Riebe M et al 2004 *Nature* **429** 734
- [59] The definition of a d -dimensional CZ gate is given by $CZ|p\rangle|q\rangle = \omega^{pq}|p\rangle|q\rangle$.
- [60] Lloyd S 1995 *Phys. Rev. Lett.* **75** 346
- [61] Bartlett S D, de Guise H and Sanders B C 2002 *Phys. Rev. A* **65** 52316
- [62] Hesse A, Köster K, Steiner J, Michl J, Vorobyov V, Dasari D, Wrachtrup J and Jendrzejewski F 2021 *New J. Phys.* **23** 023037
- [63] Endres M et al 2016 *Science* **354** 1024
- [64] Barredo D, de Léséleuc S, Lienhard V, Lahaye T and Browaeys A 2016 *Science* **354** 1021
- [65] Wang Y, Shevate S, Wintermantel T M, Morgado M, Lochead G and Whitlock S 2020 *npj Quantum Inf.* **6** 54
- [66] Muessel W, Strobel H, Linnemann D, Hume D B and Oberthaler M K 2014 *Phys. Rev. Lett.* **113** 103004
- [67] Kaufman A M, Lester B J and Regal C A 2012 *Phys. Rev. X* **2** 041014
- [68] Gross C, Strobel H, Nicklas E, Zibold T, Bar-Gill N, Kurizki G and Oberthaler M K 2011 *Nature* **480** 219
- [69] Schulze T A, Hartmann T, Voges K K, Gempel M W, Tiemann E, Zenesini A and Ospelkaus S 2018 *Phys. Rev. A* **97** 023623
- [70] Boll M, Hilker T A, Salomon G, Omran A, Nespolo J, Pollet L, Bloch I and Gross C 2016 *Science* **353** 1257
- [71] Bergschneider A, Klinkhamer V M, Becher J H, Klemt R, Palm L, Zürn G, Jochim S and Preiss P M 2019 *Nat. Phys.* **15** 640
- [72] Covey J P, Madjarov I S, Cooper A and Endres M 2019 *Phys. Rev. Lett.* **122** 173201
- [73] Kawaguchi Y and Ueda M 2012 *Phys. Rep.* **520** 253
- [74] Gottesman D, Kitaev A and Preskill J 2001 *Phys. Rev. A* **64** 012310
- [75] Knill E and Laflamme R 1997 *Phys. Rev. A* **55** 900
- [76] Mirhosseini M, Sipahigil A, Kalaei M and Painter O 2020 *Nature* **588** 599
- [77] Chamberland C et al 2020 Building a fault-tolerant quantum computer using concatenated cat codes (arXiv:2012.04108)
- [78] Fradkin E and Shenker S H 1979 *Phys. Rev. D* **19** 3682
- [79] González-Cuadra D, Zohar E and Cirac J I 2017 *New J. Phys.* **19** 063038
- [80] Van Damme M, Halimeh J C and Hauke P 2020 arXiv:2010.07338
- [81] González-Cuadra D, Bermudez A, Grzybowski P R, Lewenstein M and Dauphin A 2019 *Nat. Commun.* **10** 2694
- [82] Porras D, Ivanov P A and Schmidt-Kaler F 2012 *Phys. Rev. Lett.* **108** 235701
- [83] Nevado P and Porras D 2016 *Phys. Rev. A* **93** 13625
- [84] Kokail C et al 2019 *Nature* **569** 355
- [85] Henriët L, Beguin L, Signoles A, Lahaye T, Browaeys A, Reymond G-O and Jurczak C 2020 *Quantum* **4** 327
- [86] Argüello-Luengo J, González-Tudela A, Shi T, Zoller P and Cirac J I 2020 *Phys. Rev. Res.* **2** 042013
- [87] Aikawa K, Frisch M, Baier S, Rietzler A, Grimm R and Ferlaino F 2012 *Phys. Rev. Lett.* **108** 210401
- [88] Chalopin T, Satoor T, Evrard A, Makhalov V, Dalibard J, Lopes R and Nascimbene S 2020 *Nat. Phys.* **16** 1017
- [89] Fukuhara T, Schauß P, Endres M, Hild S, Cheneau M, Bloch I and Gross C 2013 *Nature* **502** 76
- [90] Chomaz L et al 2018 *Nat. Phys.* **14** 442
- [91] Grimsmo A L, Combes J and Baragiola B Q 2020 *Phys. Rev. X* **10** 11058
- [92] Noh K and Chamberland C 2020 *Phys. Rev. A* **101** 12316
- [93] Albert V V, Covey J P and Preskill J 2020 *Phys. Rev. X* **10** 31050
- [94] Gross J A 2020 arXiv:2005.10910
- [95] Rogel-Salazar J, New G H C, Choi S and Burnett K 2001 *J. Phys. B: At. Mol. Opt. Phys.* **34** 4617